Brain Structure and Function (2019) 224:1815–1829
https://doi.org/10.1007/s00429-019-01878-w

ORIGINAL ARTICLE

In vivo high-resolution diffusion tensor imaging of the developing neonatal rat cortex and its relationship to glial and dendritic maturation

Markus Breu[1,2,4] · Dominik Reisinger[1,2,4] · Liangcheng Tao[3] · Dan Wu[3] · Yajing Zhang[3] · Matthew D. Budde[5] · Ali Fatemi[1,2] · Arvind P. Pathak[3] · Jiangyang Zhang[6]

Received: 9 November 2018 / Accepted: 11 April 2019 / Published online: 22 April 2019

Abstract

Diffusion tensor imaging (DTI) is increasingly utilized as a sensitive tool for studying brain maturation and injuries during the neonatal period. In this study, we acquired high resolution in vivo DTI data from neonatal rat brains from postnatal day 2 (P2) to P10 and correlated temporal changes in DTI derived markers with microstructural organization of glia, axons, and dendrites during this critical period of brain development. Group average images showed dramatic temporal changes in brain morphology, fractional anisotropy (FA) and mean diffusivity (MD). Most cortical regions showed a monotonous decline in FA and an initial increase in MD from P2 to P8 that declined slightly by P10. Qualitative histology revealed rapid maturation of the glial and dendritic networks in the developing cortex. In the cingulate and motor cortex, the decreases in FA over time significantly correlated with structural anisotropy values computed from histological sections stained with glial and dendritic markers. However, in the sensory and visual cortex, other factors probably contributed to the observed decreases in FA. We did not observe any significant correlations between FA and structural anisotropy computed from the axonal histological marker.

Keywords Rat · Cortex · Development · Neonatal · Diffusion tensor imaging · Maturation · Glia

Introduction

The perinatal period is a critical phase of cortical development. Key developmental events during this period include maturation of neurons and glia as well as the formation of synaptic networks in the cortex (Bourgeois and Rakic 1993; Zecevic et al. 1989; Miller and Gauthier 2007). These immature cells and networks are susceptible to a wide range of insults, e.g., neonatal encephalopathy and systemic infections (Bourgeois and Rakic 1993; Hagberg et al. 2015; Ferriero 2004), which can lead to significant alterations in the physiological program of brain development and impacts on long-term neurological health.

Animal models are critical to our understanding of the molecular and cellular mechanisms governing perinatal cortical development and the effects of injuries during development. Previous studies on cortical development have used animal models ranging from rodents to cats and baboons (Kroenke et al. 2007; Sizonenko et al. 2007; Takahashi et al. 2011). Although models based on large animals provide better parallels to human brain development in terms of

Drs. Markus Breu and Dominik Reisinger contributed equally to this paper.

Electronic supplementary material The online version of this article (https://doi.org/10.1007/s00429-019-01878-w) contains supplementary material, which is available to authorized users.

✉ Jiangyang Zhang
jiangyang.zhang@nyumc.org

1 Division of Neurogenetics, Kennedy Krieger Institute, Baltimore, MD, USA

2 Department of Neurology, Johns Hopkins University School of Medicine, Baltimore, MD, USA

3 Department of Radiology, Johns Hopkins University School of Medicine, Baltimore, MD, USA

4 Department of Pediatrics and Adolescent Medicine, Medical University of Vienna, Vienna, Austria

5 Department of Neurosurgery, Medical College of Wisconsin, Milwaukee, WI, USA

6 Department of Radiology, New York University School of Medicine, 660 First Avenue, Room 207, New York, NY 10016, USA

gyrification, timing, and other neurophysiological aspects, rodent models have been widely used due to our extensive cellular and molecular level understanding of their development (Brazel et al. 2003; Sidman and Rakic 1973; Rakic 2009; Thompson et al. 2014). During the perinatal period, the rodent brain is at the final stage of neurogenesis (Altman and Das 1966; Feliciano and Bordey 2013) with focus on axonal and dendritic growth. The size of the brain and cortex both increased significantly with massive increases in both neuronal and non-neuronal cells (Bandeira et al. 2009). During this phase, radial glial fibers gradually degenerate and radial glial cells transform into cortical neurons (Miyata et al. 2001) and mature glia cells such as astrocytes (Semple et al. 2013; Noctor et al. 2001). Myelination in the rat cortex starts around postnatal day 10 (P10), with only traces of myelin in the corpus callosum appearing around P7 (Downes and Mullins 2014). In terms of the cellular maturation of axons, dendrites, radial glial fibers, and astrocytes, this period corresponds to the human fetal brain in its third trimester (Semple et al. 2013). Therefore, studies of neonatal rodent brain development can lead to important insights into human brain development and the effects of injuries at comparable developmental stages (Northington 2006; Vannucci and Vannucci 2005).

Non-invasive imaging techniques such as magnetic resonance imaging (MRI) have now been routinely used to examine perinatal brain injuries in the clinics (McKinstry et al. 2002b; Ment et al. 2009; Miller et al. 2002; Johnston 2003; Leigland et al. 2013). While conventional T_1 and T_2 MRI provides limited tissue contrast in the perinatal brain, diffusion MRI (Le Bihan 2003), in particular, diffusion tensor imaging (DTI) (Basser et al. 1994; Mori and Zhang 2006; Basser and Jones 2002), provides superb tissue contrasts in the fetal and neonatal human brain (Neil et al. 2002; Mukherjee et al. 2001; Lodygensky et al. 2010; Yoshida et al. 2013; Huang et al. 2006; Hermoye et al. 2006) as well as the developing rodent brain (Zhang et al. 2003; Chuang et al. 2011; Bockhorst et al. 2008; Calabrese and Johnson 2013). DTI measures the extent of water molecule diffusion restricted by the presence of microstructural tissue barriers such as axonal membranes or the directional organization of white matter fibers (Beaulieu 2002). Although more sophisticated diffusion MRI techniques such as neurite orientation dispersion and density imaging (NODDI) (Jespersen et al. 2007, 2012; Zhang et al. 2012) have been developed that provide more specific information on the cortical microstructure, their application in neonates remains limited due to lengthy acquisition and subject motion. In contrast, DTI has been increasingly used to examine the perinatal brain (Rose et al. 2015; Roze et al. 2015; van der Aa et al. 2013; Limperopoulos and Clouchoux 2009). In both humans and rodents, several reports have suggested that DTI is sensitive to the transformation of the immature radial-columnar structure (McKinstry et al. 2002a; Mori et al. 2001) to the densely connected laminar organization of the mature cortex (Neil et al. 1998; Huang et al. 2008; Kroenke et al. 2007). It was shown that both the DTI-derived mean diffusivity (MD) and fractional anisotropy (FA), which measures the extent and directional anisotropy of water diffusion, respectively, decrease as the cortex matures (Neil et al. 1998; Yoshida et al. 2013; Ball et al. 2013; Bockhorst et al. 2008). Similar trends in FA changes and regional differences have also been reported in post-mortem rat, ferret, and baboon brains (Huang et al. 2008; Kroenke et al. 2007, 2009). While it has been suggested that maturing axonal/glial/dendritic cytoarchitecture shape the spatial pattern of water diffusion from being primarily perpendicular to the cortical surface to a more heterogeneous organization (McKinstry et al. 2002a; Sizonenko et al. 2007), the correlation between changes in DTI-derived markers and cellular-level changes in the cortex during this developmental period remain to be investigated.

Several groups have studied the correlations between DTI and histological markers in the premature cortex. Sizonenko et al. showed an increase in microtubule-associated protein 2 (MAP2) staining, a marker for dendrites, and a decrease in Nestin staining, a marker for radial glial cells, in the rat cortex from P3 to P6 (Sizonenko et al. 2007). Jespersen et al. used Golgi staining to characterize the organization of axons and dendrites in the developing cortex of ferrets and reported significant correlations between FA and an anisotropy index derived from Golgi staining (Jespersen et al. 2012). Wang et al. recently examined changes in microstructural organization in the fetal rhesus monkey cortex using glial, dendritic, and axonal staining and demonstrated significant correlations between structure tensor anisotropy measured from histology and FA at two gestational stages (Wang et al. 2017).

In this study, in vivo high-resolution DTI data were acquired to characterize detailed spatiotemporal changes in FA and MD in the neonatal rat brain from P2 to P10 under normal physiological conditions. Moreover, we correlated in vivo DTI derived markers and histological markers of the microstructural organization of glia, axons, and dendrites in different cortical regions. We chose the P2–P10 period because both glial and dendritic networks undergo major remodeling while active cortical myelination is still mostly dormant. Therefore, imaging during this developmental period excludes the potential confounding effects of myelination on DTI signals. Fourier analysis (Budde et al. 2011) was used to quantitatively measure structural anisotropy of glia, axons, and dendrites from histological samples derived from the same animals. The DTI-derived metrics and histology-derived structural anisotropy were then correlated to characterize the relationship between in vivo imaging measurements and microstructural changes in these cellular components.

Materials and methods

Animals and MRI acquisition

All experimental procedures were approved by the Animal Use and Care Committee at the Johns Hopkins University School of Medicine. A total of 30 healthy neonatal Wistar rats were randomly assigned at birth for imaging at postnatal day 2 (P2), P4, P6, P8, or P10 ($n = 6$ animals for each time point). In vivo MRI was performed on a horizontal 11.7 Tesla MR scanner (Bruker Biospin, Billerica, MA, USA) with a triple-axis gradient system. Images were acquired using a quadrature volume excitation coil (72 mm diameter, for excitation) and a receive-only 4-channel phased array mouse head coil (Bruker Biospin, Billerica, MA, USA) placed on top of the head. During imaging, the rat pups were anesthetized with isoflurane (1–1.5%) together with air and oxygen mixed at a 3:1 ratio via a vaporizer. Respiration was monitored via a pressure sensor (SAII, Stony Brook, NY, USA) and maintained at 40–60 breaths per minute. After imaging, animals recovered within 5 min.

In vivo multi-slice T_2-weighted images were acquired using the rapid acquisition with relaxation enhancement (RARE) sequence with the following parameters: TE/TR = 42/6000 ms, six signal averages, FOV = 16 mm × 16 mm, a matrix size of 192 × 192, 54 slices with a slice thickness of 0.3 mm, and an imaging time of 15 min. Based on the T_2-weighted images, all animals had normal overall brain morphology without any apparent abnormalities, such as enlarged ventricles or asymmetry between the left and right hemispheres. DTI of the neonatal rat brains was performed using a modified 3D diffusion-weighted gradient and spin echo (DW-GRASE) sequence (Aggarwal et al. 2010) with the following parameters: echo time (TE)/repetition time (TR) = 28/600 ms, 2 signal averages, 20 imaging echoes (4 spin echoes distributed along the phase encoding direction and 16 gradient echoes distributed along the slice selection direction) after each excitation with twin navigator echoes in the end for motion and phase corrections, 12 diffusion directions, $b = 1000$ s/mm^2, field of view (FOV) = 16 mm × 16 mm × 16.2 mm, a matrix size of 128 × 128 × 120, and a native imaging resolution = 0.125 mm × 0.125 mm × 0.125 mm. With respiratory gating, the time for the DTI acquisition was approximately 1.5 h.

MRI data analysis

The 3D images acquired using the DW-GRASE sequence were reconstructed from raw data in MATLAB (www.mathworks.com). The twin navigator data were used to correct any phase incoherence between k space data acquired after each excitation as well as any phase incoherence between echoes acquired after the same excitation, due to subject motions or instrument instabilities as described in (Mori and van Zijl 1998). The average diffusion weighted (aDW) images were generated by computing the average of the 12 diffusion-weighted images. Using the log-linear fitting method implemented in DTIStudio (http://www.mristudio.org), the diffusion tensor was calculated for each pixel along with the apparent diffusion coefficient (ADC), fractional anisotropy (FA), and primary eigenvector. Directionally encoded colormap (DEC) images were generated by combining the FA and primary eigenvector maps, so that, at each pixel, the intensity values reflected the FA value, and the ratio of the red, green, and blue components corresponded to the x, y, and z components of the primary eigenvector. The total time for image reconstruction and DTI fitting was approximately 30 min on a desktop workstation with a 3.0 GHz CPU and 8 GB of memory. Using ROIEditor (http://www.Mristudio.org), the following regions of interest (ROIs) were manually defined in the DEC images of all the rat brains following the definitions in the Paxinos' rat brain atlas (Paxinos and Watson 2013): genu and splenium of the corpus callosum, cingulate cortex in three consecutive coronal sections, body of the corpus callosum and external capsule at five consecutive sections, the visual, auditory, sensory and motor cortices in five consecutive sections (Fig. 1). Following the protocol used by Huang et al. in postmortem rat brains (Huang et al. 2008), we further subdivided the ROIs for the sensory and motor cortices into superficial, middle, and deep layers (with equal thickness). Due to the limited spatial resolution, we were able to reliably define two layers with equal thickness (superficial and deep layers) for the visual and auditory cortices, which were thinner than the motor and sensory cortices. No subdivision of the cingulate cortex was defined as it appeared wedge-shaped in the axial images. The mean values of ADC and FA were obtained for each ROI. The time required to define ROIs for one rat brain was approximately 2 h.

For each developmental stage, group average images were generated from the 3D data using the iterative methods described in (Chuang et al. 2011; Kovacevic et al. 2005), first using intensity-based linear affine transformation and then dual channel (aDW + FA) Large Deformation Diffeomorphic Metric Mapping (LDDMM) (Ceritoglu et al. 2009) implemented in Diffeomap (http://www.mristudio.org), which took approximately 24 h on a linux cluster. FA and aDW images were used for image registration because they provide complementary contrasts that define the brain and ventricular boundaries (from the aDW images) and internal white matter tracts (from the FA images). Furthermore,

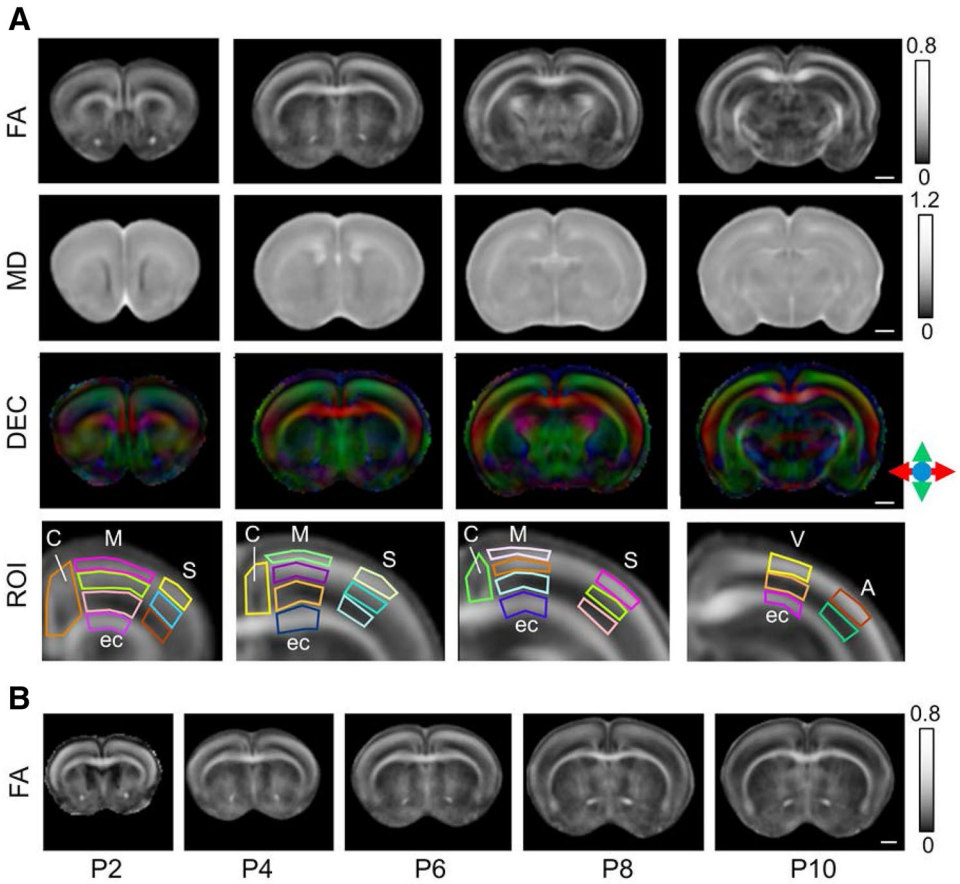

Fig. 1 Group-averaged in vivo diffusion tensor images of the developing rat brain. **a** Group-averaged FA, ADC, and directionally encoded colormap (DEC) images of the P6 rat brain at four coronal sections. The bottom row shows the superficial/middle/deep regions of interest (ROIs) used in this study. The DEC images show the estimated primary direction of tissue water diffusion, and the color scheme is: red: left–right; green: dorsal–ventral; blue: rostral-caudal as shown by the color arrows on the right. The abbreviations are: *C* cingulate cortex, *A* auditory cortex, *M* motor cortex, *S* sensory cortex, *V* visual cortex and *ec* external capsule. **b** Coronal group-averaged FA images of the rat brain from P2 to P10

mappings between group average images of the P2, P4, P6, P8, and P10 rat brains were constructed using dual channel (aDW + FA) LDDMM using the group average images of the P6 rat brains as the template, and voxel wise statistical analysis were performed across developmental stages to identify regions with significant temporal changes in ADC, FA, and local tissue volume (as measured by Log-Jacobian). We chose the P6 brain template to minimize the effects of changing cortical FA values on image mapping quality, and the mapping results showed no apparent tissue distortions. The rates of changes in these parameters over time were estimated at each pixel assuming simple linear relationships. The use of a linear model instead of more complex piecewise or nonlinear models to approximate the FA changes was justified due to the short period of time studied.

Immunohistochemistry

All animals were sacrificed after imaging. Rats were anesthetized with i.p. injections of chloral hydrate (300 mg/kg) and perfused with phosphate-buffered saline (PBS) followed by 4% formalin. The brains were extracted and fixed in formalin for 20 h followed by 24 h of 15% sucrose and 24 h of 30% sucrose. Then the brains were frozen on dry ice and sectioned at 40 μm on a cryostat. After incubation in blocking solutions, slides were incubated in primary antibody solutions overnight at 4 °C. Glial fibrillary acidic protein (Anti-GFAP Z0334, Dako, Richmond, VA, USA, 1:2500) was used for the detection of radial glia cells, microtubule associated protein 2 (Anti-MAP2, M1406, Sigma-Aldrich, St. Louis, MO, USA, 1:1000) for the detection of dendrites, and Anti-Pan-Axonal Neurofilament Marker (SMI-312R, Covance, Princeton, NJ, USA, 1:2000) for the detection of axons. Antibody binding was visualized using an ABC ELITE kit (Vector Labs, Burlingame, CA, USA) and DAB reaction.

Brain sections were imaged using a Zeiss Axio Imager microscope (Zeiss Microimaging, LLC, Thornwood, NY, USA) with bright-field imaging under standardized illumination and image acquisition settings. Z-stack images were acquired with optical sections of 5 μm each and were taken under a 20× objective in anatomically selected areas corresponding to the cortical ROIs defined in MRI data. Z layers were collapsed using Zeiss Axiovision's wavelet algorithm and mosaic images were stitched together using Zeiss Axiovision software. Bright-field images were exported as loss-free compressed TIFF files to MCID Core (InterFocus Imaging Ltd., Cambridge, UK).

Fourier analysis of histological data

Fourier analysis was performed on histological images to generate microscopic anisotropy measurements as described in (Budde et al. 2011). Briefly, a moving 200 pixel × 200 pixel (~ 0.1 mm × 0.1 mm) window was used to extract data from the histological images, the window moved along the horizontal or vertical axes with a step size of 20 pixels. Intensity values within the 200 × 200 window were filtered by a Tukey window ($\alpha = 0.4$) and normalized to zero mean before 2D Fourier transformation, after which a radial histogram was calculated as described in (Budde et al. 2011). Using principle component analysis, the directional anisotropy in 2D, called "structural anisotropy" (SA) here, was calculated from the two eigenvalues (λ_1 and λ_2, with λ_1 greater or equal to λ_2) of the covariance matrix based on the radial histogram as $SA = 1 - \lambda_2/\lambda_1$. For more details, please see (Budde et al. 2011). The maps of SA and the mean intensity values within the moving windows were then used for ROI-based analysis. Similar ROIs as defined in the MRI data were manually drawn on the original histological images and down-sampled to the maps of microstructural anisotropy and mean intensity maps to obtain the mean.

Statistical analysis

Pearson correlation coefficients were computed using linear regression to describe decreases in FA between P2 and P10. A Kruskal–Wallis test with correction for multiple comparisons was used to compare values between the time points. For each ROI, linear regression was performed between the mean intensity and structural anisotropy values from GFAP, MAP2, and SMI-312 stained histological sections and DTI-derived FA and MD values in the matching ROI. Statistical analyses of ROI data were performed with Prism 6 (GraphPad Software, Inc. La Jolla, CA, USA). p values of < 0.05 were considered significant. Voxel-based regressions of FA, MD, and Jacobian values were performed using Matlab (Mathworks.com) with corrections for multiple comparisons (the false discovery rate was set at 0.05).

Results

In vivo DTI of the neonatal rat cortex

Group averaged FA images of the P6 rat cortex (Fig. 1a) revealed a superficial (external) portion with relatively high diffusion anisotropy and a deep (internal) portion with low diffusion anisotropy. This pattern was consistent throughout the rostral and caudal cortices, although the superficial portion with high FA tended to be larger in the rostral than in the caudal cortex. In the ADC maps, no clear distinction between the superficial and deep cortex was observed. The primary directions of water diffusion in the high FA portion of the cortex, as visualized by the directionally encoded colormap (DEC) images, were mostly along the radial direction, perpendicular to the cortical surface. Group averaged diffusion tensor images from P2 to P10 rat brains (Fig. 1b) further showed consistent radial patterns but gradual reductions in FA in the superficial cortex over time. To examine this inhomogeneity of cortical anisotropy, we placed multiple cortical ROIs at five sections along the rostrocaudal axis (Fig. 1a, ROI) as described by Huang et al. (2008). For each cortical region except the cingulate cortex, we defined two or three ROIs (superficial, middle, and deep) with equal thickness in the FA images.

Regional changes in structural volumes and diffusion measurements

ROI-based analyses showed significant reductions in FA from P2 to P10 in most cortical ROIs, but no apparent change in the selected subcortical white areas (Fig. 2a and Table 1). Results of linear regression suggested that the superior layers had stronger correlations between their FA values and postnatal stage than the deep layers (Fig. 2a). Cortical MD values generally showed significant increases from P2 to P8 followed by a slight decrease by P10 (Fig. 2b and Table 2). The decreases in MD values were significant in the superior layers of the motor and sensory cortices and the deep layer of the visual cortex (Table 2). Due to these non-monotonic changes in MD values, linear fitting was not performed. In the corpus callosum, no significant change in FA was detected over the same period, but a significant increase in MD was detected in the body of the corpus callosum (bcc, $p = 0.0006$).

Voxel-based regression analysis showed significant temporal changes in FA, MD, and local tissue volume throughout the brain (Fig. 3). From P2 to P10, the estimated rate of FA reduction was greater in the superficial layers in the sensory and visual cortices than other parts of the forebrain. From P2 to P8, significant increases in MD were found in the superficial portions of the motor, sensory, and visual cortices, as well as in the striatum and external capsule. From P2 to P10, most brain regions showed significant growth in volumes, with the cingulate cortex, superficial layer of the motor and sensory cortices, striatum, and external capsule showing more rapid expansion than other regions.

Histological examination of the neonatal rat cortical development and structural anisotropy analysis

GFAP, MAP2, and SMI-312 stained sections of the neonatal rat cortex showed radial organization patterns (Fig. 4). Structural anisotropy (SA) generated from these sections

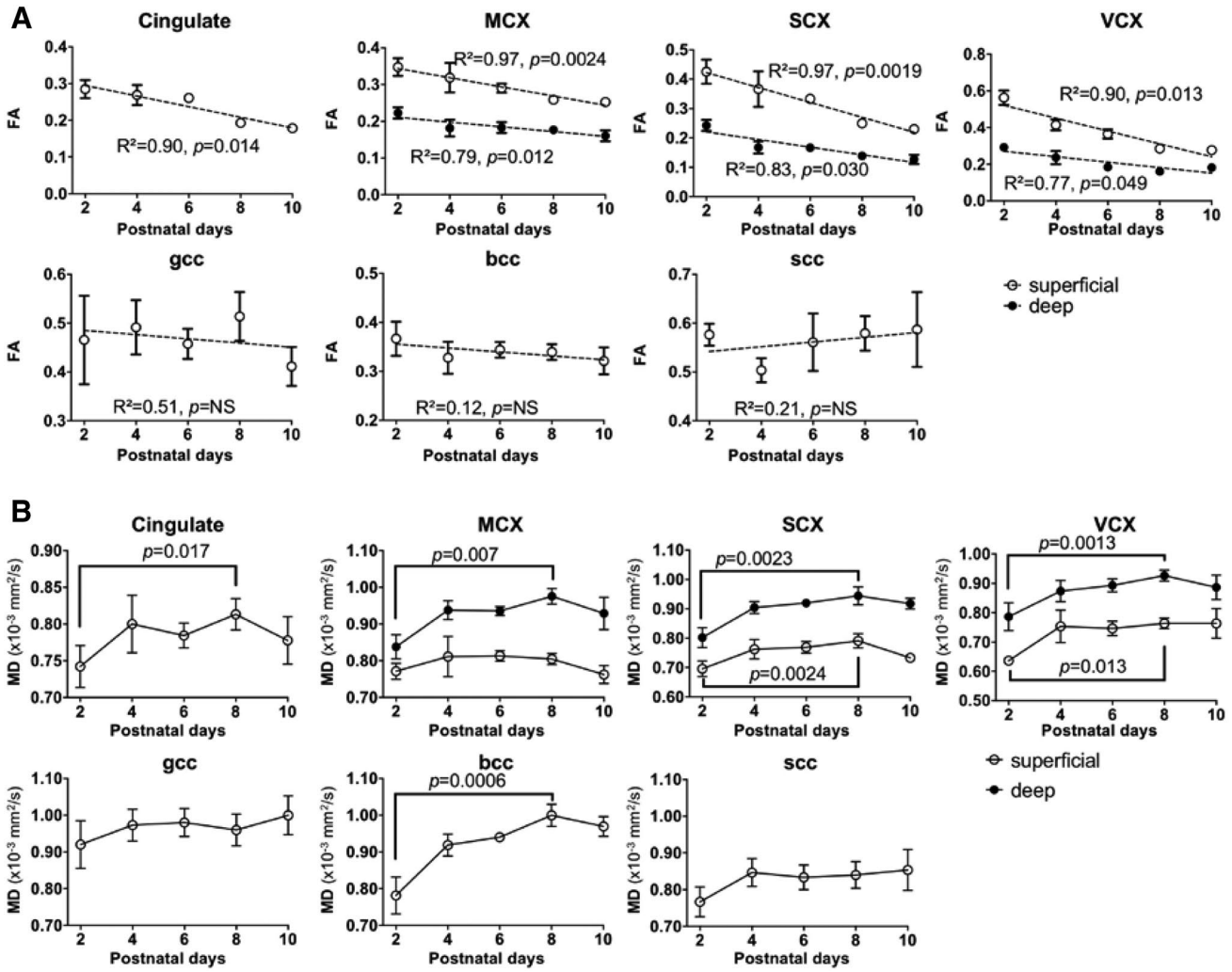

Fig. 2 Time dependent FA and MD changes from P2 to P10 in selected ROIs. **a** FA changes in cortical and subcortical ROIs. The dashed lines show the results of linear regression. **b** MD changes in cortical and subcortical ROIs. Kruskal–Wallis test, corrected for multiple comparison. The abbreviations are: *MCX* motor cortex, *SCX* sensory cortex, *VCX* visual cortex, *bcc/gcc/scc* body/genu/splenium of the corpus callosum. Error bars indicate SDs

Table 1 FA values of several cortical regions in the developing rat brain from P2 to P10

Ages	Cingulate	MCX		SCX		VCX	
		Superficial	Deep	Superficial	Deep	Superficial	Deep
P2	0.28 ± 0.02	0.35 ± 0.02	0.22 ± 0.01	0.43 ± 0.04	0.24 ± 0.02	0.56 ± 0.04	0.29 ± 0.01
P4	0.27 ± 0.02	0.32 ± 0.04	0.18 ± 0.02	0.37 ± 0.05	0.17 ± 0.02	0.41 ± 0.03	0.24 ± 0.03
P6	0.26 ± 0.01	0.29 ± 0.01	0.18 ± 0.01	0.33 ± 0.01	0.17 ± 0.01	0.36 ± 0.02	0.18 ± 0.01
P8	0.19 ± 0.01	0.26 ± 0.01*	0.18 ± 0.01	0.25 ± 0.01*	0.14 ± 0.01*	0.29 ± 0.01*	0.16 ± 0.01*
P10	0.18 ± 0.01*	0.25 ± 0.01*	0.16 ± 0.01*	0.23 ± 0.01*	0.13 ± 0.01*	0.28 ± 0.01*	0.18 ± 0.02*

Mean and standard deviation values are shown

*Indicates significant change ($p < 0.05$, Kruskal–Wallis test with corrections for multiple comparisons) from P2

could sensitively detect anisotropic organization of stained cellular processes. The corpus callosum and external capsule had higher SA values than the cortex, due to the dense and orderly organization of structures there. Subtle features in the cortical microstructural organization could also be detected in the SA maps. In the GFAP stained section, the

Table 2 MD values of several cortical regions in the developing rat brain from P2 to P10

Ages	Cingulate	MCX		SCX		VCX	
		Superficial	Deep	Superficial	Deep	Superficial	Deep
P2	0.74 ± 0.03	0.77 ± 0.02	0.84 ± 0.03	0.70 ± 0.02	0.80 ± 0.03	0.64 ± 0.01	0.79 ± 0.04
P4	0.80 ± 0.04	0.81 ± 0.05	0.94 ± 0.02	0.76 ± 0.03	0.90 ± 0.02	0.75 ± 0.05	0.87 ± 0.03
P6	0.78 ± 0.02	0.81 ± 0.01	0.94 ± 0.01	0.77 ± 0.02	0.92 ± 0.01	0.75 ± 0.02	0.89 ± 0.02
P8	0.81 ± 0.02*	0.80 ± 0.01	0.98 ± 0.02*	0.79 ± 0.02*	0.94 ± 0.03*	0.76 ± 0.02*	0.93 ± 0.02*
P10	0.78 ± 0.03	0.76 ± 0.02**	0.93 ± 0.04	0.73 ± 0.01**	0.92 ± 0.02	0.76 ± 0.05	0.89 ± 0.04

The unit is $\times 10^{-3}$ mm^2/s

Mean and standard deviation values are shown

*Indicates that the value is significantly different from the corresponding value at P2 ($p < 0.05$, Kruskal–Wallis test with corrections for multiple comparisons)

**Indicates that the value is significantly different from the corresponding value at P8 ($p < 0.05$, Kruskal–Wallis test with corrections for multiple comparisons)

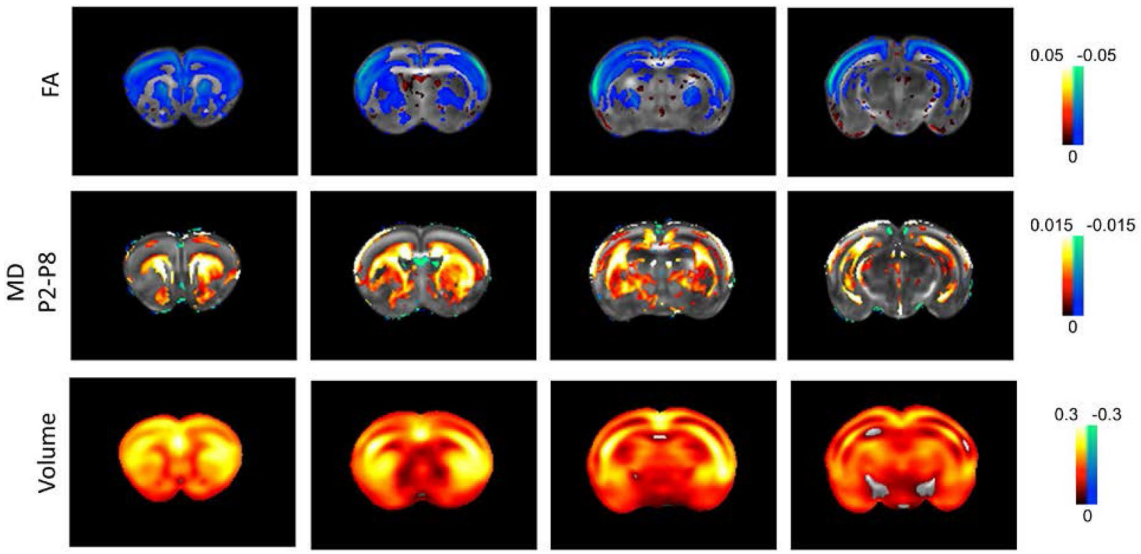

Fig. 3 Voxel-wise estimation of the rates of FA and MD as well as local tissue volume changes. Only voxels with significant change are shown here. The color scheme uses blue to green to indicate the rate of decline in values and red to yellow to indicate the rate of increase in values. Corrections for multiple comparisons were performed for the voxel-based analysis with false discovery rates less than 0.05. The unit for the rate of FA or volume change is 1/day, and the unit for the rate of MD change is $mm^2/s/day$

region just beneath the cortical surface (region 1 in Fig. 4) showed more radially organized processes than the mid cortex (region 2), and the SA maps showed higher SA in region 1 than region 2. In the MAP2 stained sections, the motor cortex (region 1) showed more densely organized processes radial to the cortical surface than the cingulate cortex (region 2), and the SA maps showed higher SA in the motor cortex than the cingulate cortex. In the SMI-312 stained sections, neuronal bodies were stained in the superficial portion of the cortex (region 1), whereas the axons were more easily identified in the deep portion (region 2). In comparison, the SA map showed slightly higher SA in the deep portion than the superficial portion.

At P2, GFAP stained sections showed prominent radial glia fibers reaching from subcortical areas to the cortical surface. Figure 5a shows representative sections from the cingulate cortex and motor cortex. Throughout the cortical layer there were some interspersed immature astrocytes, and clusters of immature cells could be distinguished in internal cortical areas. At P10 only remains of the radial glia cell scaffold could be discerned, whereas an isotropic network of astrocytes had formed. Quantitative analysis showed no apparent change in the mean intensity of GFAP staining throughout the cortex. SA based on GFAP showed significant time-related decreases in the cingulate cortex and the superficial portion of the motor cortex (Fig. 5a). Several

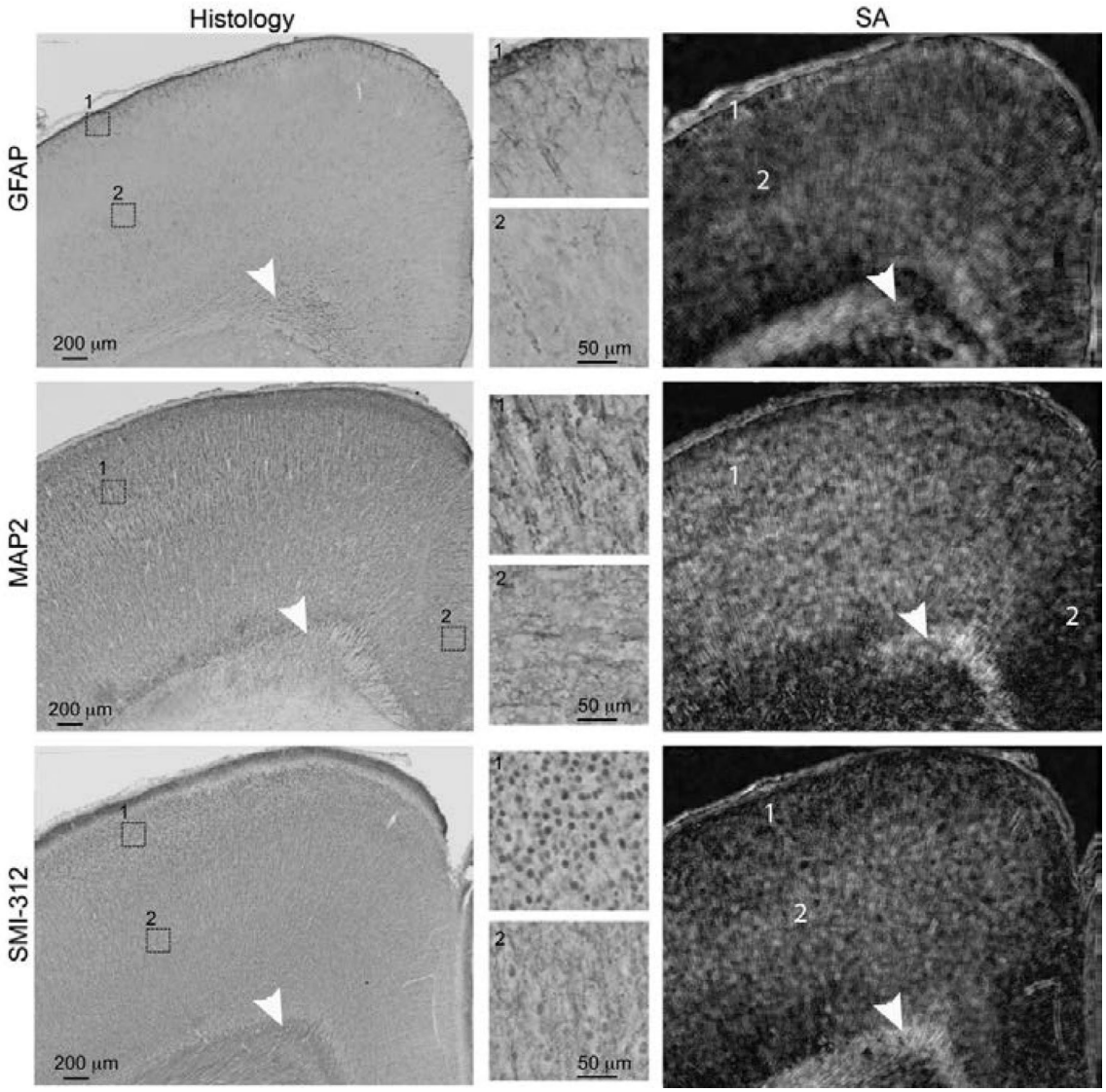

Fig. 4 Comparison of immunohistochemistry (GFAP, MAP2, SMI-312) and corresponding SA maps of a P6 frontal cortex. White arrows indicate the locations of subcortical white matter structures. Distinct spatial patterns of cellular processes in selected regions in the histological sections (inside boxes 1 and 2) are enlarged to show the spatial patterns of cellular processes

other cortical regions also showed significant decreases in SA from P2 to P10, including the motor cortex (deep layer; $R^2 = 0.86$, $p = 0.024$), sensory cortex (deep layer; $R^2 = 0.80$, $p = 0.040$, Fig. S2 in the supplementary materials), and visual cortex (deep layer, $R^2 = 0.88$, $p = 0.018$, Fig. S1 in the supplementary materials). Other cortical regions did not show significant changes in GFAP-based SA (as shown in Figs. S1 and S2 in the supplementary materials).

At P2, MAP2 immunostaining showed thick radially oriented tract-like structures. At P10, the radial orientation was still visible, but less pronounced. Quantitative analysis showed no apparent change in the mean intensity of MAP2 staining throughout the cortex. SA based on MAP2 stained sections, however, showed significant time-related decreases in the cingulate cortex and deep portion of the motor cortex (Fig. 5b). Other regions that showed significant decreases in SA included the motor cortex (superficial layer; $R^2 = 0.84$, $p = 0.029$) and visual cortex (superficial layer; $R^2 = 0.78$, $p = 0.046$, Fig. S1 in the supplementary materials). SA based on SMI-312 stained sections showed significant time-related decreased SA values in the cingulate cortex ($R^2 = 0.98$, $p = 0.011$, Fig. S3 in the supplementary materials), whereas portion of the sensory cortex showed significant increases in SA values (deep layer; $R^2 = 0.95$, $p = 0.0047$). No overall change in the mean intensity of SMI-312 staining was observed in the cortex.

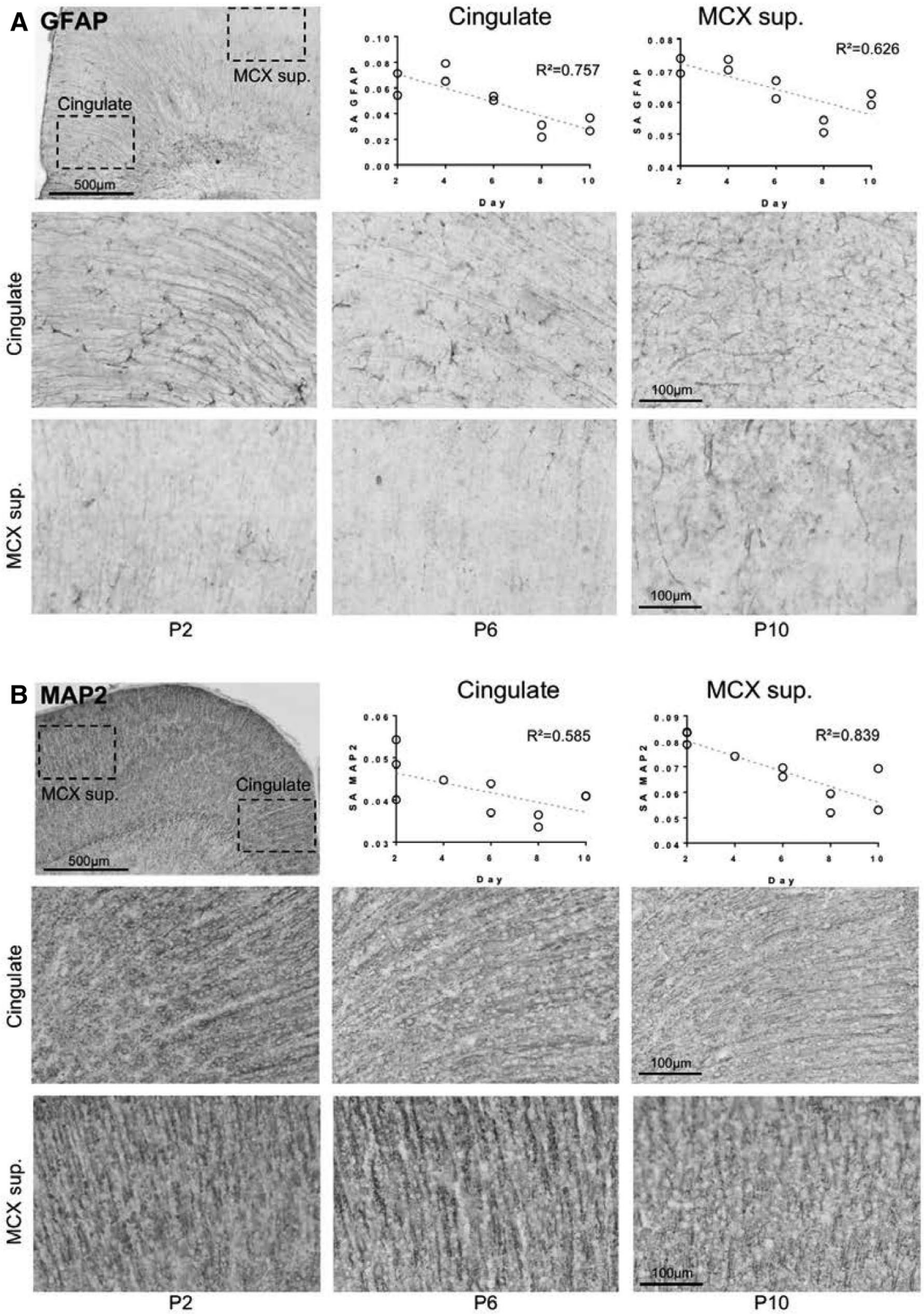

Fig. 5 Temporal changes in SA from GFAP (**a**) and MAP2 (**b**) stained sections containing the cingulate cortex and superficial portion of the motor cortex at P2, P6, and P10. Note the development of dense radial fibers at P2 to a more diffuse fiber orientation at P10 in the enlarged images

Correlations between histology and DTI-based anisotropy measurements

In the cingulate cortex, the FA significantly correlated with the SA values from GFAP-based histology (Fig. 6, $R^2 = 0.656$, $p = 0.0045$). In the motor cortex, the superficial layer FA values correlated significantly with SA from MAP2-stained histology ($R^2 = 0.7773$, $p = 0.0007$). Other areas that showed correlations include the superficial layer of motor cortex with anisotropy from GFAP stained histology ($R^2 = 0.5953$, $p = 0.0089$), and the superficial layer of visual cortex with anisotropy from MAP2 stained histology ($R^2 = 0.5659$, $p = 0.0121$). SMI-312-stained histology did not show any significant correlation with MRI-based measurements. No significant correlation was observed between the mean intensity of histology and FA or MD values. In comparison, there was only a marginal correlation between MD and SMI-312 SA values in the superficial layer of the motor cortex (Fig. 7a). Several other cortical regions also showed significant correlations potentially due to an outlier at P2 (Fig. 7).

Discussion

In this study, we used in vivo high-resolution DTI to examine the spatial patterns of cortical FA and MD values and follow their temporal changes in several cortical regions of the neonatal rat. As the cortex consists of several layers, each with distinct cellular microstructural organization, high-resolution data can potentially distinguish layer specific microstructural patterns. 3D high-resolution imaging data with isotropic spatial resolution can also facilitate mapping of spatiotemporal changes during cortical development using a common template as shown in Fig. 3.

The study focused on a short neonatal period (P2–P10), before the start of myelination processes in most brain regions, with a relatively high temporal resolution (every 2 days). The ability to acquire in vivo diffusion MRI signals allowed us to examine tissue properties under normal physiological conditions compared to post-mortem studies, in which tissue properties can be altered by cell death and chemical fixation (Shepherd et al. 2009). For instance, ex vivo MD values are significantly lower than in vivo measurements (Zhang et al. 2011; Sun et al. 2003). Although several studies have shown that FA values of normal white matter tracts in adult mouse brains from ex vivo DTI are comparable to in vivo measurements (Sun et al. 2003),

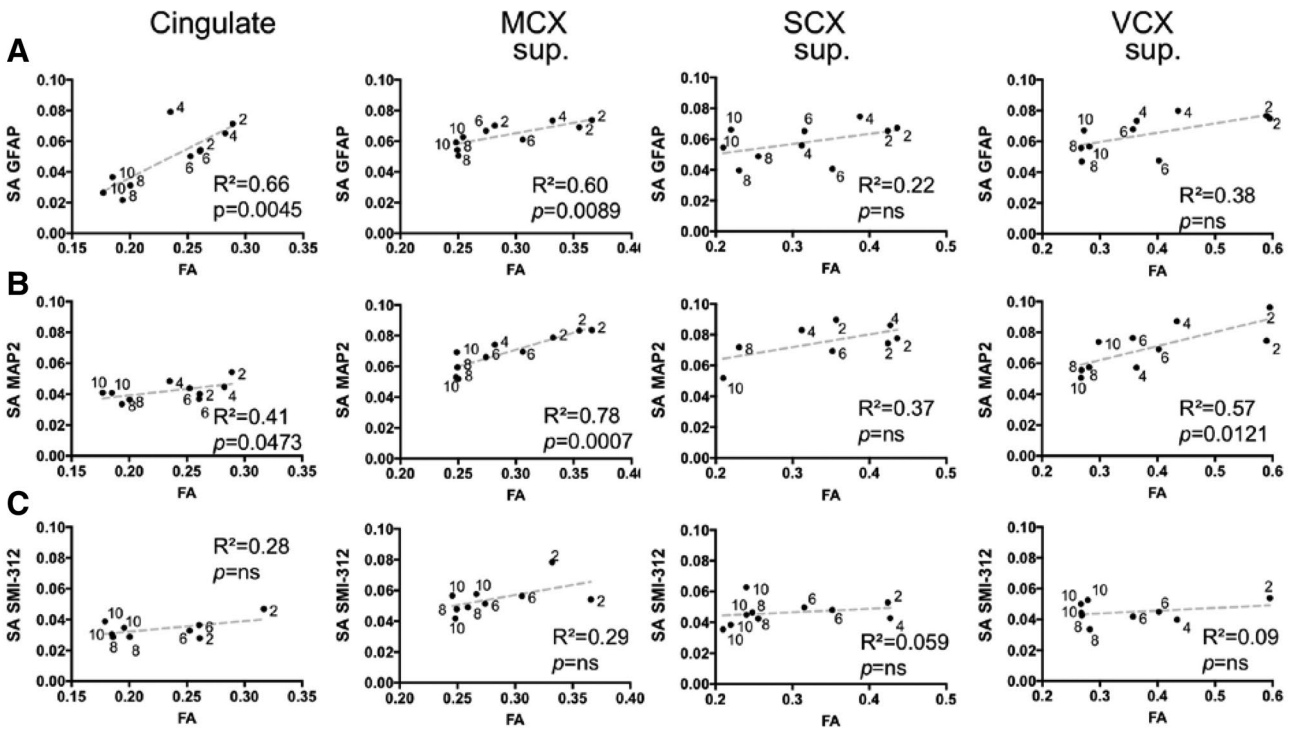

Fig. 6 Correlations between SA and FA. **a** Correlation between SA from GFAP staining and FA. **b** Correlation between SA from MAP2 staining and FA. **c** Correlation between SA from SMI-312 staining and FA. The labels next to the symbols indicate the age

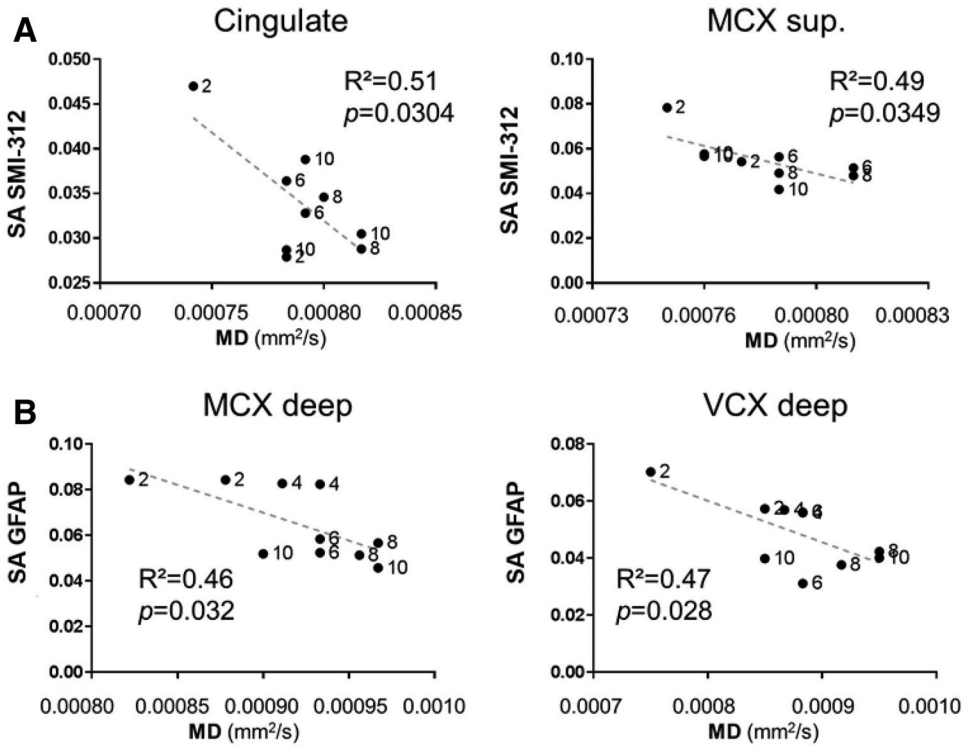

Fig. 7 Correlations between cortical MD and SA. **a** Correlation between MD and SA from SMI-312 staining. **b** Correlation between MD and SA from GFAP staining

ex vivo FA values can deviate from in vivo FA values under certain pathological conditions (Sun et al. 2006). Due to the potential neurotoxicity associated with repeated exposure to isoflurane or other anesthetic agents (Zanghi and Jevtovic-Todorovic 2017), we did not adopt a longitudinal study design, but instead performed a cross-sectional study with the benefit that MRI and histological data from the same animals could be directly correlated.

The high-resolution in vivo imaging data enabled us to map regional differences in the in cortical FA and MD over time. Consistent with two previous studies of post-mortem rat brains (Huang et al. 2008; Calabrese and Johnson 2013) and one in vivo study (Bockhorst et al. 2008), significant decreases of FA were observed in most superficial cortical regions from P2 to P10 (Fig. 2). A recent report on time-dependent changes in FA in preterm and normal infants (Ball et al. 2013) also showed that the rates of FA changes were not homogeneous, with the prefrontal, sensory association, and visual association cortices showing more rapid reductions in FA than other cortical regions at 28–40 post-conceptional weeks. Although it is difficult to directly compare observations from the rat brain with those from the human brain, the observed relationships between the DTI-derived markers and cortical cyto-architectural changes may provide important insights for human studies.

The voxel-based results (Fig. 3), which mapped the extents and locations of FA changes, further demonstrated that the superficial portion of the sensory and visual cortices exhibited the most rapid reductions in FA values, and the cingulate and superficial layer of the motor cortex showed moderate reductions in FA values. The results, however, depended on the accuracy of image registration, and the observed significant changes in cortical FA values over time certainly posed a challenge. From P2 to P10, changes in FA values of major white matter tracts (e.g., the corpus callosum) were relatively small (Fig. 2a) as suggested by previous studies (Bockhorst et al. 2008; Calabrese and Johnson 2013), probably due to the lack of active myelination during this time period. With relatively stable white matter contrast in FA maps and the use of the P6 brains as template, our mapping results showed no apparent mis-registration within cortical regions. For studies that involve altered brain development or injuries, with potential changes in brain morphology and tissue contrasts, image registration results should be examined carefully to avoid such confounding factors.

Interestingly, we found significant increases in MD values between P2 and P8 in several internal cortical regions, followed by gradual decreases from P8 to P10. Previously, Bockhorst et al. (Bockhorst et al. 2008) reported a similar initial increase in cortical MD values followed by a prolonged decline from P8 to approximately P30. Most previous studies in humans only showed monotonic decreases in cortical MD values over time, e.g. (Ball et al. 2013), however, McKinstry et al. reported initial increases in cortical MD values, which peaked at approximately 33 weeks, followed by decreases in MD values afterwards (McKinstry et al. 2002a). These studies attributed the decrease in MD to the formation of densely interconnected mature

cortical networks, including dendrites, synapses (Ball et al. 2013), and myelination (Bockhorst et al. 2008), but it was not clear what caused the early increases in cortical MD values. In our study, we did not find robust correlations between MD and glia and dendritic markers, which suggest that increases in MD were not directly related to degeneration of the radial glia scaffold or increased dendritic arborization.

The increases in cortical MD values may reflect a rapid decrease of neuronal density in the neonatal rat cortex. Previously, Bandeira et al. studied the numbers of neuronal and non-neuronal cells in the developing rat brain (Bandeira et al. 2009). Their results showed that, during the first week of postnatal development, the neuronal density in the rat cortex decreased significantly by more than fourfold, whereas the number of non-neuronal cells increased mostly during the second and third week. This timing of changing neuronal numbers and density during the first week agrees well with our MRI findings. Our results showed that the superficial portion of the sensory and visual cortices had both faster increases in MD and decreases in FA than most other cortical regions (Fig. 3). It is possible that the rapid increases in MD in these regions reflect active decreases in neuronal density, which may also contribute to the declines of FA values.

Several groups have quantitatively examined the relationships between cortical FA values with underlying tissue microstructures via structural tensor analysis or similar methods, e.g., (Budde and Annese 2013; Budde and Frank 2012; Wang et al. 2017; Salo et al. 2017). In particular, Wang et al. (Wang et al. 2017) showed in fetal monkey brains that FA values correlated with structural tensor based anisotropy values from Vimentin (a glial marker) and MAP2 stained sections but not from SMI-312 stained sections, which agrees with our results from the neonatal rat brain (Fig. 5). Fourier analysis has also been used to study microstructural organizations, in particular the orientation and directional anisotropy in comparison with DTI results, in the monkey and rat brains (Budde et al. 2011; Choe et al. 2012). Compared to structural tensor analysis, results of Fourier analysis are of lower spatial resolution but sufficient for comparison with the DTI data. Current evidence suggests that two processes likely contribute to the decreases in FA between P2 and P10 in the cingulate and motor cortices (superficial layer): (1) the transition from the radial glial fiber scaffold to an isotropic glial network, and (2) dendritic arborization. In contrast, no significant temporal change in GFAP and MAP2 SA values was detected in the superficial layers of the sensory and visual cortices (Figs. S1 and S2), although they showed the most rapid declines in FA values. Since Fourier analysis may not capture all the microstructural changes in glial, dendritic, and axonal networks, the origins of the FA changes in these two regions remain to be investigated further.

It is necessary to mention some of the limitations of this study. First, DTI cannot resolve complex microstructural organization, e.g., crossing of axons or dendrites, which is common in the cortex, even at prenatal and neonatal stages. The ability to resolve crossing fibers may allow us to better characterize the cortical axonal and dendritic networks. More sophisticated diffusion MRI methods than DTI (Frank 2001; Tuch et al. 2002; Wedeen et al. 2005; Jespersen et al. 2007, 2012; Zhang et al. 2012) have been developed to resolve crossing fibers or quantify neurite density, which are important for studying cortical development. However, these techniques require lengthy acquisition times, which is challenging for in vivo studies at high spatial resolution. Second, the ability of the histological markers used in this study to bind to target structures and their biological distributions may vary during cortical development. Third, the histological images and analysis in this study were two dimensional, whereas the DTI results reflect water diffusion in three dimensional cortical tissues. Therefore, their correlations may not capture their exact relationship. Even though we do not expect cortical microstructural organization to change drastically along the rostral-caudal direction compared to the other two directions within the resolution of the DTI acquisition (0.125 mm), 3D microstructural information from serial confocal images, as shown in recent reports (Schilling et al. 2016; Khan et al. 2015), would provide more complete information on microstructural changes in the developing cortex. Recent development in other imaging modalities, such as 3D polarized light imaging (Axer et al. 2011; Mollink et al. 2017) and 3D Fourier analysis of 3D electron microscopy (EM) data (Salo et al. 2018), may also benefit future studies in this area.

In summary, our results demonstrate the spatiotemporal changes in FA and MD in neonatal rat cortex from P2 to P10. We found significant increases in MD in several cortical regions from P2 to P8 without any significant correlations between MD and histological markers used in this study. In contrast, in the cingulate and motor cortex, the decreases in FA over time were significantly correlated with structural anisotropy values from histological sections stained with glial and dendritic markers. However, in the sensory and visual cortex, other factors probably contribute to the decreases in FA. Future studies that utilize more sophisticated diffusion MRI and microscopy techniques with a wider array of histological markers (e.g. markers for myelination and neurons) may reveal the exact link between diffusion MRI-based markers and the evolving microstructural landscape in the developing cortex. Such knowledge in both normal developing brains and models of early brain injuries, such as inflammation or hypoxia ischemia, will pave the way to better use of diffusion MRI-based markers in the clinics.

Acknowledgements This study is funded by National Institute of Neurological Disorders and Stroke (Grant No. R01NS102904) and National Institute of Child Health and Human Development (Grant No. R01HD074593).

Compliance with ethical standards

Conflict of interest The authors have no conflict of interest.

Ethical approval All experimental procedures were approved by the Animal Use and Care Committee at the Johns Hopkins University School of Medicine. This study did not involve human subjects. This work was supported by the National Institutes of Health R01HD074593 and R01NS102904.

References

Aggarwal M, Mori S, Shimogori T, Blackshaw S, Zhang J (2010) Three-dimensional diffusion tensor microimaging for anatomical characterization of the mouse brain. Magn Reson Med 64(1):249–261. https://doi.org/10.1002/mrm.22426

Altman J, Das GD (1966) Autoradiographic and histological studies of postnatal neurogenesis: I. A longitudinal investigation of the kinetics, migration and transformation of cells incorporating tritiated thymidine in neonate rats, with special reference to postnatal neurogenesis in some brain regions. J Comp Neurol 126(3):337–389. https://doi.org/10.1002/cne.901260302

Axer M, Amunts K, Grassel D, Palm C, Dammers J, Axer H, Pietrzyk U, Zilles K (2011) A novel approach to the human connectome: ultra-high resolution mapping of fiber tracts in the brain. NeuroImage 54(2):1091–1101. https://doi.org/10.1016/j.neuroimage.2010.08.075

Ball G, Srinivasan L, Aljabar P, Counsell SJ, Durighel G, Hajnal JV, Rutherford MA, Edwards AD (2013) Development of cortical microstructure in the preterm human brain. Proc Natl Acad Sci USA 110(23):9541–9546. https://doi.org/10.1073/pnas.1301652110

Bandeira F, Lent R, Herculano-Houzel S (2009) Changing numbers of neuronal and non-neuronal cells underlie postnatal brain growth in the rat. Proc Natl Acad Sci USA 106(33):14108–14113. https://doi.org/10.1073/pnas.0804650106

Basser PJ, Jones DK (2002) Diffusion-tensor MRI: theory, experimental design and data analysis—a technical review. NMR Biomed 15(7–8):456–467. https://doi.org/10.1002/nbm.783

Basser PJ, Mattiello J, LeBihan D (1994) MR diffusion tensor spectroscopy and imaging. Biophys J 66(1):259–267. https://doi.org/10.1016/S0006-3495(94)80775-1

Beaulieu C (2002) The basis of anisotropic water diffusion in the nervous system—a technical review. NMR Biomed 15(7–8):435–455. https://doi.org/10.1002/nbm.782

Bockhorst KH, Narayana PA, Liu R, Ahobila-Vijjula P, Ramu J, Kamel M, Wosik J, Bockhorst T, Hahn K, Hasan KM, Perez-Polo JR (2008) Early postnatal development of rat brain: in vivo diffusion tensor imaging. J Neurosci Res 86(7):1520–1528. https://doi.org/10.1002/jnr.21607

Bourgeois JP, Rakic P (1993) Changes of synaptic density in the primary visual cortex of the macaque monkey from fetal to adult stage. J Neurosci 13(7):2801–2820

Brazel CY, Romanko MJ, Rothstein RP, Levison SW (2003) Roles of the mammalian subventricular zone in brain development. Prog Neurobiol 69(1):49–69

Budde MD, Annese J (2013) Quantification of anisotropy and fiber orientation in human brain histological sections. Front Integr Neurosci 7:3. https://doi.org/10.3389/fnint.2013.00003

Budde MD, Frank JA (2012) Examining brain microstructure using structure tensor analysis of histological sections. NeuroImage 63(1):1–10. https://doi.org/10.1016/j.neuroimage.2012.06.042

Budde MD, Janes L, Gold E, Turtzo LC, Frank JA (2011) The contribution of gliosis to diffusion tensor anisotropy and tractography following traumatic brain injury: validation in the rat using Fourier analysis of stained tissue sections. Brain 134(Pt 8):2248–2260. https://doi.org/10.1093/brain/awr161

Calabrese E, Johnson GA (2013) Diffusion tensor magnetic resonance histology reveals microstructural changes in the developing rat brain. NeuroImage 79:329–339. https://doi.org/10.1016/j.neuroimage.2013.04.101

Ceritoglu C, Oishi K, Li X, Chou MC, Younes L, Albert M, Lyketsos C, van Zijl PC, Miller MI, Mori S (2009) Multi-contrast large deformation diffeomorphic metric mapping for diffusion tensor imaging. NeuroImage 47(2):618–627. https://doi.org/10.1016/j.neuroimage.2009.04.057

Choe AS, Stepniewska I, Colvin DC, Ding Z, Anderson AW (2012) Validation of diffusion tensor MRI in the central nervous system using light microscopy: quantitative comparison of fiber properties. NMR Biomed 25(7):900–908. https://doi.org/10.1002/nbm.1810

Chuang N, Mori S, Yamamoto A, Jiang H, Ye X, Xu X, Richards LJ, Nathans J, Miller MI, Toga AW, Sidman RL, Zhang J (2011) An MRI-based atlas and database of the developing mouse brain. NeuroImage 54(1):80–89. https://doi.org/10.1016/j.neuroimage.2010.07.043

Downes N, Mullins P (2014) The development of myelin in the brain of the juvenile rat. Toxicol Pathol 42(5):913–922. https://doi.org/10.1177/0192623313503518

Feliciano DM, Bordey A (2013) Newborn cortical neurons: only for neonates? Trends Neurosci 36(1):51–61. https://doi.org/10.1016/j.tins.2012.09.004

Ferriero DM (2004) Neonatal brain injury. N Engl J Med 351(19):1985–1995. https://doi.org/10.1056/NEJMra041996

Frank LR (2001) Anisotropy in high angular resolution diffusion-weighted MRI. Magn Reson Med 45(6):935–939

Hagberg H, Mallard C, Ferriero DM, Vannucci SJ, Levison SW, Vexler ZS, Gressens P (2015) The role of inflammation in perinatal brain injury. Nat Rev Neurol 11(4):192–208. https://doi.org/10.1038/nrneurol.2015.13

Hermoye L, Saint-Martin C, Cosnard G, Lee SK, Kim J, Nassogne MC, Menten R, Clapuyt P, Donohue PK, Hua K, Wakana S, Jiang H, van Zijl PC, Mori S (2006) Pediatric diffusion tensor imaging: normal database and observation of the white matter maturation in early childhood. NeuroImage 29(2):493–504. https://doi.org/10.1016/j.neuroimage.2005.08.017

Huang H, Zhang J, Wakana S, Zhang W, Ren T, Richards LJ, Yarowsky P, Donohue P, Graham E, van Zijl PC, Mori S (2006) White and gray matter development in human fetal, newborn and pediatric brains. NeuroImage 33(1):27–38. https://doi.org/10.1016/j.neuroimage.2006.06.009

Huang H, Yamamoto A, Hossain MA, Younes L, Mori S (2008) Quantitative cortical mapping of fractional anisotropy in developing rat brains. J Neurosci 28(6):1427–1433. https://doi.org/10.1523/JNEUROSCI.3194-07.2008

Jespersen SN, Kroenke CD, Ostergaard L, Ackerman JJ, Yablonskiy DA (2007) Modeling dendrite density from magnetic resonance diffusion measurements. NeuroImage 34(4):1473–1486. https://doi.org/10.1016/j.neuroimage.2006.10.037

Jespersen SN, Leigland LA, Cornea A, Kroenke CD (2012) Determination of axonal and dendritic orientation distributions within the developing cerebral cortex by diffusion tensor imaging.

IEEE Trans Med Imaging 31(1):16–32. https://doi.org/10.1109/TMI.2011.2162099
Johnston MV (2003) MRI for neonatal encephalopathy in full-term infants. Lancet 361(9359):713–714
Khan AR, Cornea A, Leigland LA, Neuroimage K-SG (2015) 3D structure tensor analysis of light microscopy data for validating diffusion MRI. NeuroImage 111:192–203
Kovacevic N, Henderson JT, Chan E, Lifshitz N, Bishop J, Evans AC, Henkelman RM, Chen XJ (2005) A three-dimensional MRI atlas of the mouse brain with estimates of the average and variability. Cereb Cortex 15(5):639–645. https://doi.org/10.1093/cercor/bhh165
Kroenke CD, Van Essen DC, Inder TE, Rees S, Bretthorst GL, Neil JJ (2007) Microstructural changes of the baboon cerebral cortex during gestational development reflected in magnetic resonance imaging diffusion anisotropy. J Neurosci 27(46):12506–12515. https://doi.org/10.1523/JNEUROSCI.3063-07.2007
Kroenke CD, Taber EN, Leigland LA, Knutsen AK, Bayly PV (2009) Regional patterns of cerebral cortical differentiation determined by diffusion tensor MRI. Cereb Cortex 19(12):2916–2929. https://doi.org/10.1093/cercor/bhp061
Le Bihan D (2003) Looking into the functional architecture of the brain with diffusion MRI. Nat Rev Neurosci 4(6):469–480. https://doi.org/10.1038/Nrn1119
Leigland LA, Budde MD, Cornea A, Kroenke CD (2013) Diffusion MRI of the developing cerebral cortical gray matter can be used to detect abnormalities in tissue microstructure associated with fetal ethanol exposure. NeuroImage 83:1081–1087. https://doi.org/10.1016/j.neuroimage.2013.07.068
Limperopoulos C, Clouchoux C (2009) Advancing fetal brain MRI: targets for the future. Semin Perinatol 33(4):289–298. https://doi.org/10.1053/j.semperi.2009.04.002
Lodygensky GA, Vasung L, Sizonenko SV, Huppi PS (2010) Neuroimaging of cortical development and brain connectivity in human newborns and animal models. J Anat 217(4):418–428. https://doi.org/10.1111/j.1469-7580.2010.01280.x
McKinstry RC, Mathur A, Miller JH, Ozcan A, Snyder AZ, Schefft GL, Almli CR, Shiran SI, Conturo TE, Neil JJ (2002a) Radial organization of developing preterm human cerebral cortex revealed by non-invasive water diffusion anisotropy MRI. Cereb Cortex 12(12):1237–1243
McKinstry RC, Miller JH, Snyder AZ, Mathur A, Schefft GL, Almli CR, Shimony JS, Shiran SI, Neil JJ (2002b) A prospective, longitudinal diffusion tensor imaging study of brain injury in newborns. Neurology 59(6):824–833
Ment LR, Hirtz D, Huppi PS (2009) Imaging biomarkers of outcome in the developing preterm brain. Lancet Neurol 8(11):1042–1055. https://doi.org/10.1016/S1474-4422(09)70257-1
Miller FD, Gauthier AS (2007) Timing is everything: making neurons versus glia in the developing cortex. Neuron 54(3):357–369. https://doi.org/10.1016/j.neuron.2007.04.019
Miller S, Ferriero D, Barkovich AJ, Silverstein F (2002) Practice parameter: neuroimaging of the neonate: report of the Quality Standards Subcommittee of the American Academy of Neurology and the Practice Committee of the Child Neurology Society. Neurology 59(10):1663 **(author reply 1663–1664)**
Miyata T, Kawaguchi A, Okano H, Ogawa M (2001) Asymmetric inheritance of radial glial fibers by cortical neurons. Neuron 31(5):727–741
Mollink J, Kleinnijenhuis M, Cappellen van Walsum AV, Sotiropoulos SN, Cottaar M, Mirfin C, Heinrich MP, Jenkinson M, Pallebage-Gamarallage M, Ansorge O, Jbabdi S, Miller KL (2017) Evaluating fibre orientation dispersion in white matter: comparison of diffusion MRI, histology and polarized light imaging. NeuroImage 157:561–574. https://doi.org/10.1016/j.neuroimage.2017.06.001
Mori S, van Zijl PC (1998) A motion correction scheme by twin-echo navigation for diffusion-weighted magnetic resonance imaging with multiple RF echo acquisition. Magn Reson Med 40(4):511–516
Mori S, Zhang J (2006) Principles of diffusion tensor imaging and its applications to basic neuroscience research. Neuron 51(5):527–539. https://doi.org/10.1016/j.neuron.2006.08.012
Mori S, Itoh R, Zhang J, Kaufmann WE, van Zijl PC, Solaiyappan M, Yarowsky P (2001) Diffusion tensor imaging of the developing mouse brain. Magn Reson Med 46(1):18–23
Mukherjee P, Miller JH, Shimony JS, Conturo TE, Lee BC, Almli CR, McKinstry RC (2001) Normal brain maturation during childhood: developmental trends characterized with diffusion-tensor MR imaging. Radiology 221(2):349–358. https://doi.org/10.1148/radiol.2212001702
Neil JJ, Shiran SI, McKinstry RC, Schefft GL, Snyder AZ, Almli CR, Akbudak E, Aronovitz JA, Miller JP, Lee BC, Conturo TE (1998) Normal brain in human newborns: apparent diffusion coefficient and diffusion anisotropy measured by using diffusion tensor MR imaging. Radiology 209(1):57–66. https://doi.org/10.1148/radiology.209.1.9769812
Neil J, Miller J, Mukherjee P, Huppi PS (2002) Diffusion tensor imaging of normal and injured developing human brain—a technical review. NMR Biomed 15(7–8):543–552. https://doi.org/10.1002/nbm.784
Noctor SC, Flint AC, Weissman TA, Dammerman RS, Kriegstein AR (2001) Neurons derived from radial glial cells establish radial units in neocortex. Nature 409(6821):714–720. https://doi.org/10.1038/35055553
Northington FJ (2006) Brief update on animal models of hypoxic-ischemic encephalopathy and neonatal stroke. ILAR J 47(1):32–38
Paxinos G, Watson C (2013) The rat brain in stereotaxic coordinates, 7th edn. Academic Press, New York
Rakic P (2009) Evolution of the neocortex: a perspective from developmental biology. Nat Rev Neurosci 10(10):724–735. https://doi.org/10.1038/nrn2719
Rose J, Cahill-Rowley K, Vassar R, Yeom KW, Stecher X, Stevenson DK, Hintz SR, Barnea-Goraly N (2015) Neonatal brain microstructure correlates of neurodevelopment and gait in preterm children 18–22 month of age: an MRI and DTI study. Pediatr Res 78(6):700–708. https://doi.org/10.1038/pr.2015.157
Roze E, Benders MJ, Kersbergen KJ, van der Aa NE, Groenendaal F, van Haastert IC, Leemans A, de Vries LS (2015) Neonatal DTI early after birth predicts motor outcome in preterm infants with periventricular hemorrhagic infarction. Pediatr Res 78(3):298–303. https://doi.org/10.1038/pr.2015.94
Salo RA, Miettinen T, Laitinen T, Grohn O, Sierra A (2017) Diffusion tensor MRI shows progressive changes in the hippocampus and dentate gyrus after status epilepticus in rat—histological validation with Fourier-based analysis. NeuroImage 152:221–236. https://doi.org/10.1016/j.neuroimage.2017.03.003
Salo RA, Belevich I, Manninen E, Jokitalo E, Grohn O, Sierra A (2018) Quantification of anisotropy and orientation in 3D electron microscopy and diffusion tensor imaging in injured rat brain. NeuroImage 172:404–414. https://doi.org/10.1016/j.neuroimage.2018.01.087
Schilling K, Janve V, Gao Y, Stepniewska I, Landman BA, Anderson AW (2016) Comparison of 3D orientation distribution functions measured with confocal microscopy and diffusion MRI. NeuroImage 129:185–197
Semple BD, Blomgren K, Gimlin K, Ferriero DM, Noble-Haeusslein LJ (2013) Brain development in rodents and humans: identifying benchmarks of maturation and vulnerability to injury across species. Prog Neurobiol 106–107:1–16. https://doi.org/10.1016/j.pneurobio.2013.04.001

Shepherd TM, Thelwall PE, Stanisz GJ, Blackband SJ (2009) Aldehyde fixative solutions alter the water relaxation and diffusion properties of nervous tissue. Magn Reson Med 62(1):26–34. https://doi.org/10.1002/mrm.21977

Sidman RL, Rakic P (1973) Neuronal migration, with special reference to developing human brain: a review. Brain Res 62(1):1–35

Sizonenko SV, Camm EJ, Garbow JR, Maier SE, Inder TE, Williams CE, Neil JJ, Huppi PS (2007) Developmental changes and injury induced disruption of the radial organization of the cortex in the immature rat brain revealed by in vivo diffusion tensor MRI. Cereb Cortex 17(11):2609–2617. https://doi.org/10.1093/cercor/bhl168

Sun SW, Neil JJ, Song SK (2003) Relative indices of water diffusion anisotropy are equivalent in live and formalin-fixed mouse brains. Magn Reson Med 50(4):743–748. https://doi.org/10.1002/mrm.10605

Sun SW, Liang HF, Le TQ, Armstrong RC, Cross AH, Song SK (2006) Differential sensitivity of in vivo and ex vivo diffusion tensor imaging to evolving optic nerve injury in mice with retinal ischemia. NeuroImage 32(3):1195–1204. https://doi.org/10.1016/j.neuroimage.2006.04.212

Takahashi E, Dai G, Rosen GD, Wang R, Ohki K, Folkerth RD, Galaburda AM, Wedeen VJ, Ellen Grant P (2011) Developing neocortex organization and connectivity in cats revealed by direct correlation of diffusion tractography and histology. Cereb Cortex 21(1):200–211. https://doi.org/10.1093/cercor/bhq084

Thompson CL, Ng L, Menon V, Martinez S, Lee CK, Glattfelder K, Sunkin SM, Henry A, Lau C, Dang C, Garcia-Lopez R, Martinez-Ferre A, Pombero A, Rubenstein JLR, Wakeman WB, Hohmann J, Dee N, Sodt AJ, Young R, Smith K, Nguyen TN, Kidney J, Kuan L, Jeromin A, Kaykas A, Miller J, Page D, Orta G, Bernard A, Riley Z, Smith S, Wohnoutka P, Hawrylycz MJ, Puelles L, Jones AR (2014) A high-resolution spatiotemporal atlas of gene expression of the developing mouse brain. Neuron 83(2):309–323. https://doi.org/10.1016/j.neuron.2014.05.033

Tuch DS, Reese TG, Wiegell MR, Makris N, Belliveau JW, Wedeen VJ (2002) High angular resolution diffusion imaging reveals intravoxel white matter fiber heterogeneity. Magn Reson Med 48(4):577–582. https://doi.org/10.1002/mrm.10268

van der Aa NE, Northington FJ, Stone BS, Groenendaal F, Benders MJ, Porro G, Yoshida S, Mori S, de Vries LS, Zhang J (2013) Quantification of white matter injury following neonatal stroke with serial DTI. Pediatr Res 73(6):756–762. https://doi.org/10.1038/pr.2013.45

Vannucci RC, Vannucci SJ (2005) Perinatal hypoxic-ischemic brain damage: evolution of an animal model. Dev Neurosci 27(2–4):81–86. https://doi.org/10.1159/000085978

Wang X, Studholme C, Grigsby PL, Frias AE, Cuzon Carlson VC, Kroenke CD (2017) Folding, but not surface area expansion, is associated with cellular morphological maturation in the fetal cerebral cortex. J Neurosci 37(8):1971–1983. https://doi.org/10.1523/JNEUROSCI.3157-16.2017

Wedeen VJ, Hagmann P, Tseng WY, Reese TG, Weisskoff RM (2005) Mapping complex tissue architecture with diffusion spectrum magnetic resonance imaging. Magn Reson Med 54(6):1377–1386. https://doi.org/10.1002/mrm.20642

Yoshida S, Oishi K, Faria AV, Mori S (2013) Diffusion tensor imaging of normal brain development. Pediatr Radiol 43(1):15–27. https://doi.org/10.1007/s00247-012-2496-x

Zanghi CN, Jevtovic-Todorovic V (2017) A holistic approach to anesthesia-induced neurotoxicity and its implications for future mechanistic studies. Neurotoxicol Teratol 60:24–32. https://doi.org/10.1016/j.ntt.2016.12.004

Zecevic N, Bourgeois JP, Rakic P (1989) Changes in synaptic density in motor cortex of rhesus monkey during fetal and postnatal life. Brain Res Dev Brain Res 50(1):11–32

Zhang J, Richards LJ, Yarowsky P, Huang H, van Zijl PC, Mori S (2003) Three-dimensional anatomical characterization of the developing mouse brain by diffusion tensor microimaging. NeuroImage 20(3):1639–1648

Zhang J, Jones MV, McMahon MT, Mori S, Calabresi PA (2011) In vivo and ex vivo diffusion tensor imaging of cuprizone-induced demyelination in the mouse corpus callosum. Magn Reson Med. https://doi.org/10.1002/mrm.23032

Zhang H, Schneider T, Wheeler-Kingshott CA, Alexander DC (2012) NODDI: practical in vivo neurite orientation dispersion and density imaging of the human brain. NeuroImage 61(4):1000–1016. https://doi.org/10.1016/j.neuroimage.2012.03.072